Oxygen dynamics in the aftermath of the Great Oxidation of Earth's atmosphere

Donald E. Canfield[a,1], Lauriss Ngombi-Pemba[b], Emma U. Hammarlund[a], Stefan Bengtson[c], Marc Chaussidon[d], François Gauthier-Lafaye[e], Alain Meunier[b], Armelle Riboulleau[f], Claire Rollion-Bard[d], Olivier Rouxel[g], Dan Asael[g], Anne-Catherine Pierson-Wickmann[h], and Abderrazak El Albani[b]

[a]Nordic Center for Earth Evolution (NordCEE), and Institute of Biology, University of Southern Denmark, DK-5230 Odense M, Denmark; [b]Institut de Chimie des Milieux et Matériaux de Poitiers, Unité Mixte de Recherche 7285, Centre National de la Recherche Scientifique-Institut National des Sciences de l'Univers-Institut National de chimie, Université de Poitiers, 86000 Poitiers, France; [c]Department of Palaeozoology, Swedish Museum of Natural History, SE-104 05 Stockholm, Sweden; [d]Centre de Recherches Pétrographiques et Géochimiques, Centre National de la Recherche Scientifique, Unité Propre de Recherche 2300, 54501 Vandoeuvre-lès-Nancy, France; [e]Laboratoire d'Hydrologie et de Géochimie de Strasbourg, Unité Mixte de Recherche 7517, Centre National de la Recherche Scientifique, 67084 Strasbourg, France; [f]Laboratoire Géosystèmes, Unité Mixte de Recherche 8217, Centre National de la Recherche Scientifique, Université Lille 1, 59655 Villeneuve d'Ascq, France; [g]Institut Français de la Recherche pour l'Exploitation de la Mer (IFREMER), Centre de Brest, Technopôle Brest-Iroise, 29280 Plouzané, France; and [h]Département Géosciences, Unité Mixte de Recherche 6118, Université de Rennes, 35042 Rennes, France

Contributed by Donald E. Canfield, August 29, 2013 (sent for review July 2, 2013)

The oxygen content of Earth's atmosphere has varied greatly through time, progressing from exceptionally low levels before about 2.3 billion years ago, to much higher levels afterward. In the absence of better information, we usually view the progress in Earth's oxygenation as a series of steps followed by periods of relative stasis. In contrast to this view, and as reported here, a dynamic evolution of Earth's oxygenation is recorded in ancient sediments from the Republic of Gabon from between about 2,150 and 2,080 million years ago. The oldest sediments in this sequence were deposited in well-oxygenated deep waters whereas the youngest were deposited in euxinic waters, which were globally extensive. These fluctuations in oxygenation were likely driven by the comings and goings of the Lomagundi carbon isotope excursion, the longest–lived positive $\delta^{13}C$ excursion in Earth history, generating a huge oxygen source to the atmosphere. As the Lomagundi event waned, the oxygen source became a net oxygen sink as Lomagundi organic matter became oxidized, driving oxygen to low levels; this state may have persisted for 200 million years.

GOE | Paleoproterozoic | marine chemistry | Mo isotope | trace metal

Multiple lines of geochemical evidence (1–4) point to a substantial increase in the oxygen content of the atmosphere some 2,300–2,400 million years ago (Ma) in what is known as the "Great Oxidation Event" (GOE) (4). This rise in oxygen occurred during an episode of major glaciation, known as the Huronian glaciation, but the cause of oxygen increase remains elusive. Some have argued that the GOE occurred as a direct result of cyanobacterial evolution (5) whereas others have assumed that cyanobacteria evolved well before the GOE and have looked for causes involving changes in the redox balance of the Earth surface (6–9). In any event, beginning after the GOE, and sometime between 2,300 and 2,230 Ma, there was a large positive excursion in the ^{13}C of marine inorganic carbon that was apparently global in nature (10–13). This event is known as the Lomagundi carbon isotope excursion, with $\delta^{13}C$ values reaching upwards of 12 per mil. The event lasted well over 100 million years, with a termination estimated at between about 2,110 Ma and 2,080 Ma and no later than 2,060 Ma (10, 14). This excursion represents the largest positive carbon-isotope excursion in Earth history.

In standard thinking, a large positive carbon-isotope excursion is driven by the enhanced burial of organic carbon into sediments (15, 16). An event as sustained and dramatic as the Lomagundi excursion would seemingly require an unusual driving mechanism, and it has been suggested that the GOE itself may have been the cause through enhanced oxidative weathering on land accompanying the increase in oxygen. This oxidative weathering liberated more phosphorus to the oceans and stimulated primary production and organic carbon burial (17, 18). Organic carbon burial is a source of oxygen to the atmosphere, and it also has been suggested that the Lomagundi excursion may have driven atmospheric oxygen to higher levels than attained during the GOE itself (17, 19). The deposition of massive calcium sulfate deposits during the Lomagundi Event (20–22), indicating elevated seawater sulfate concentrations, would be consistent with this increase in oxygen. Also, the concentrations of uranium in shales deposited in anoxic marine waters during the Lomagundi excursion show enrichment compared with shales deposited both before and after the excursion (23). This observation would indicate higher marine U concentrations, consistent with globally expanded oxic conditions in marine waters. However, when ratioed to total organic carbon (TOC), the biggest U enrichments are found within the Huronian glaciation, during the initiation of the GOE, whereas the enrichments during the Lomagundi excursion are much smaller and quite comparable to those found before the GOE (23) when atmospheric oxygen was much lower in concentration (1, 3). Therefore, there remain some uncertainties in interpreting the U signal.

There also have been some suggestions that oxygen fell again to lower levels as the Lomagundi event waned (17, 24, 25). Of particular interest here is an increase in the isotopic composition in $\delta^{34}S$ of carbonate associated sulfate (CAS) through the Lomagundi event, which could be taken to indicate an expansion of euxinic conditions (24) as might be expected with falling oxygen levels. However, although consistent with lower levels of ocean oxygenation, this isotope data is not direct evidence, and

Significance

The Great Oxidation of Earth's atmosphere about 2.3 billion years ago began a series of geochemical events leading to elevated oxygen levels for the next 200 million years, with a collapse to much lower levels as these events played their course. This sequence of events is represented in rocks from the Republic of Gabon. We show oxygenation of the deep oceans when oxygen levels were likely their highest. By 2.08 billion years ago, however, oxygen dropped to levels possibly as low as any time in the last 2.3 billion years. These fluctuations can be explained as a direct consequence of the initial oxygenation of the atmosphere during the Great Oxidation Event.

Author contributions: A.E.A. headed the project; D.E.C., L.N.-P., E.U.H., S.B., O.R., and A.E.A. designed research; L.N.-P., E.U.H., M.C., F.G.-L., A.M., A.R., C.R.-B., O.R., D.A., A.-C.P.-W., and A.E.A. performed research; D.E.C., L.N.-P., E.U.H., and A.E.A. analyzed data; and D.E.C., L.N.-P., E.U.H., and A.E.A. wrote the paper.

The authors declare no conflict of interest.

[1]To whom correspondence should be addressed. E-mail: dec@biology.sdu.dk.

This article contains supporting information online at www.pnas.org/lookup/suppl/doi:10.1073/pnas.1315570110/-/DCSupplemental.

the CAS results are apparently restricted to sediments deposited during the Lomagundi event (as evidenced by elevated $\delta^{13}C$ values) and not afterward. Overall, although there are compelling reasons to believe that the Lomagundi excursion, and its aftermath, represented a dynamic period in the history of Earth oxygenation, there is little direct evidence for the state of atmospheric and ocean oxygenation both during and beyond the event. This time window is also represented by the Francevillian Group of Gabon. Here, we explore the nature of marine water-column chemistry during the deposition of these rocks, providing a unique window into the evolution of ocean and atmospheric chemistry during what appears as an exceptionally dynamic period of oxygen evolution in Earth history.

The Francevillian Basin

The Francevillian Basin is composed of 35,000 km^2 of unmetamorphosed sedimentary rocks deposited during the Paleoproterozoic Eon in an epicontinental setting in what is now the Republic of Gabon, located in western equatorial Africa. The sediment package is between 1,000 and 2,500 m thick, and it is subdivided into five lithostratigraphic units, FA to FE, which rest unconformably on Archean basement rocks (26) (Fig. 1). The FA unit consists of mainly fluviatile and deltaic sandstones, and, at the top, it contains uranium enrichments and the well-known Oklo nuclear reactors (27). After a period of rifting and basin deepening, the deep-water marine-dominated sediments of the FB unit began to deposit. These sediments were deposited below the storm wave base. Due to its complex lithology, the FB unit is further divided into the FB1 (a, b, and c) and FB2 (a and b) subunits. The FB1a and FB1b subunits consist of mixed shales, sandstones, and conglomerates, fining upwards to predominantly shales at the top. This is a regressive sequence. Sea level began to rise again near the bottom of the FB1c subunit, reaching maximum depth below the storm wave base with deposition of a thin iron formation in the middle of the subunit. The bottom of the FB1c subunit, in turn, is overlain by black shales and a thick Mn-rich sediment package. After the deposition of the iron formation, sea level dropped through the deposition of the FB2 subunit, which consists of sandstone beds deposited in channels near the fair-weather wave base. These sandstones are sharply overlain by finely laminated black shales interbedded with thin siltstone layers deposited by waning storm surge (FB2b). It is from here that large colonial organisms have previously been reported (28). Stromatolites are found in topographic highs at the base of the FC formation (29), after which the overlying black shales of the FD formation were deposited in a transgressive phase. Diagenetic illites from the top of the FB1b subunit yield a Sm-Nd age of 2,099 ± 115 Ma (30) whereas a more precise U-Pb age of 2,083 ± 6 Ma is reported from a welded tuff near the top of the FD unit (31). In addition, a Rb-Sr age of 2,143 ± 143 Ma is reported for coarse-grained syenites of the N'Goutou alkaline massive, which is interlaid with rocks at the base of the FB1 subunit (32). Overall, the bulk of these Gabon rocks were deposited during the Lomagundi isotope excursion.

We collected both core material and fresh outcrop samples from the base of the FB1 subunit to the middle of the FD unit (see *SI Text* for details). We subjected these to a range of geochemical analyses with the goal of understanding the evolution of water chemistry both during and in the aftermath of the Lomagundi isotope excursion. Our analyses included concentration determinations of a number of major elements (Fe, Mn, S, Al), organic carbon, and a variety of trace metals (U, Mo, V), as well as isotope analyses for reduced sulfur, organic carbon, molybdenum, and a full suite of Fe speciation determinations. All of these bear on understanding the redox history of the waters in

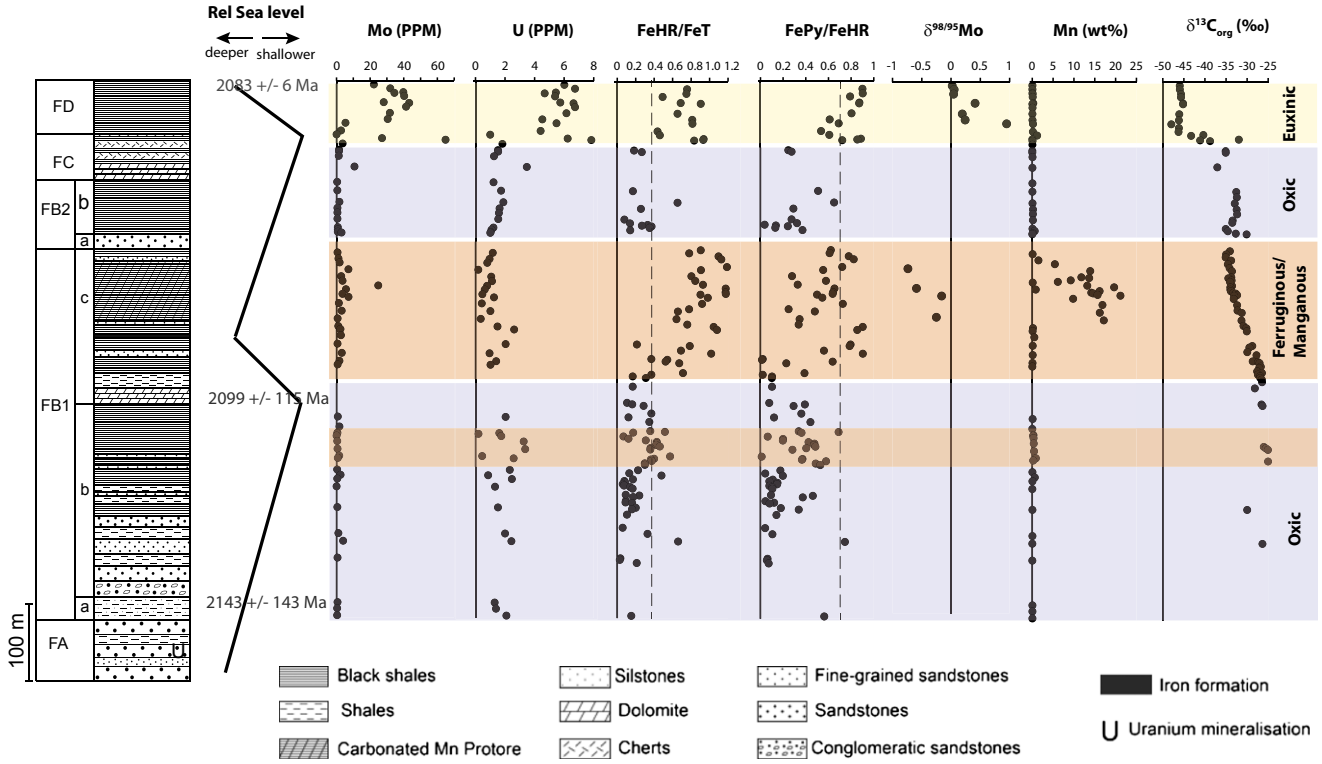

Fig. 1. Distribution of the elements and isotopes in Francevillian sediments used to reconstruct depositional environment (see also Fig. S1 for additional data), as also indicated on the figure. There may be a thin ferruginous interval near the top of the FB1b subunit as indicated. A reconstruction of relative sea-level trends is also shown as well as available chronological constraints.

the Francevillian Basin, as well as global seawater. The methods are outlined in *SI Text*.

Results and Discussion

Placing the Fracevillian Sequence in the Context of the Lomagundi Excursion. Carbonates are too scarce in Francevillian rocks to allow direct comparison with the Lomagundi excursion, but these rocks can be placed within the excursion through a comparison of organic carbon isotope values (33). Thus, our organic carbon isotope analyses (Fig. 1; see Table S2 for full list of data), similar to previous determinations from the Francevillian of Gabon (34), show the beginning of a decrease in $\delta^{13}C$ at the base of the FB1c unit, with a further decrease through the FC unit with quite depleted values (down to −46 per mil) in the FD unit. These data can be compared with the coupled inorganic and organic carbon isotope record from the contemporaneous Fennoscandia of Arctic Russia (33), showing that the Lomagundi event began before the deposition of the Francevillian sequence. The event was in full force during the deposition of subunits FB1a and FB1b and appears to wane in the middle of the Francevillian subunit FB1c (Fig. 1), in concert with the initial fall in organic carbon $\delta^{13}C$ values (Fig. 1). However, elevated $\delta^{13}C$ values from shallow-water dolomites from the FC unit would be consistent with the Lomagundi event persisting until the bottom 1/3 of the FC unit (21). As in Fennoscandia, we observe large depletions in the $\delta^{13}C$ of organic carbon in the FD unit dated at 2,086 ± 6 Ma (see *The Francevillian Basin*). In Fennoscandia, the ^{13}C-depleted organic carbon is associated within so-called shungite deposits (see *SI Text* and Table S1). These are a noncrystalline form of carbon believed to represent fossilized oil with carbon contents of up to 99% (35). The age of these deposits is constrained between 1,980 ± 27 Ma and 2,090 ± 70 Ma, with a preliminary Re-Os age of 2,050 Ma (uncertainty not given) on the shungites themselves (33, 35). Shungite deposition therefore postdates the Lomagundi excursion, and available age constraints allow the placement of the Francevillian FD unit as contemporaneous with shungite deposition (33). The FD unit is thus also most likely post-Lomagundi.

The highly depleted ^{13}C values from both Fennoscandia and Gabon have been previously interpreted to reflect the weathering of Lomagundi organic carbon into the global inorganic carbon pool (33). In this view, the Lomagundi excursion was accompanied by an unusually large burial flux of ^{13}C-depleted organic carbon. This organic carbon became available for oxidative weathering to inorganic carbon when these Lomagundi-aged sediments were delivered into the weathering zone, providing an unusually large flux of ^{13}C-depleted carbon to the oceans (33). In an alternative hypothesis, it has been argued that the $\delta^{13}C$ of organic matter within the FB (and perhaps also FC) has been locally influenced by the incorporation of ^{13}C-depleted methanotroph-derived organic matter (36). We cannot completely rule out this possibility, but the large organic matter excursion as observed through the upper FC unit and into the FD is likely a global feature expressed in Gabon, Fennoscandia, and perhaps elsewhere (35).

Fe Speciation and Trace Metals. Fe speciation results are also presented in Fig. 1. We have focused our sampling to fine-grained sedimentary rocks and the chemical sediments of the banded iron formation (BIF) and Mn-rich layers free of any obvious hydrothermal or late diagenetic overprint. We have also analyzed some chert and carbonate rocks, but we have not focused on these as low Fe and low clastic contents might compromise the reliability of Fe speciation and metal enrichment interpretations.

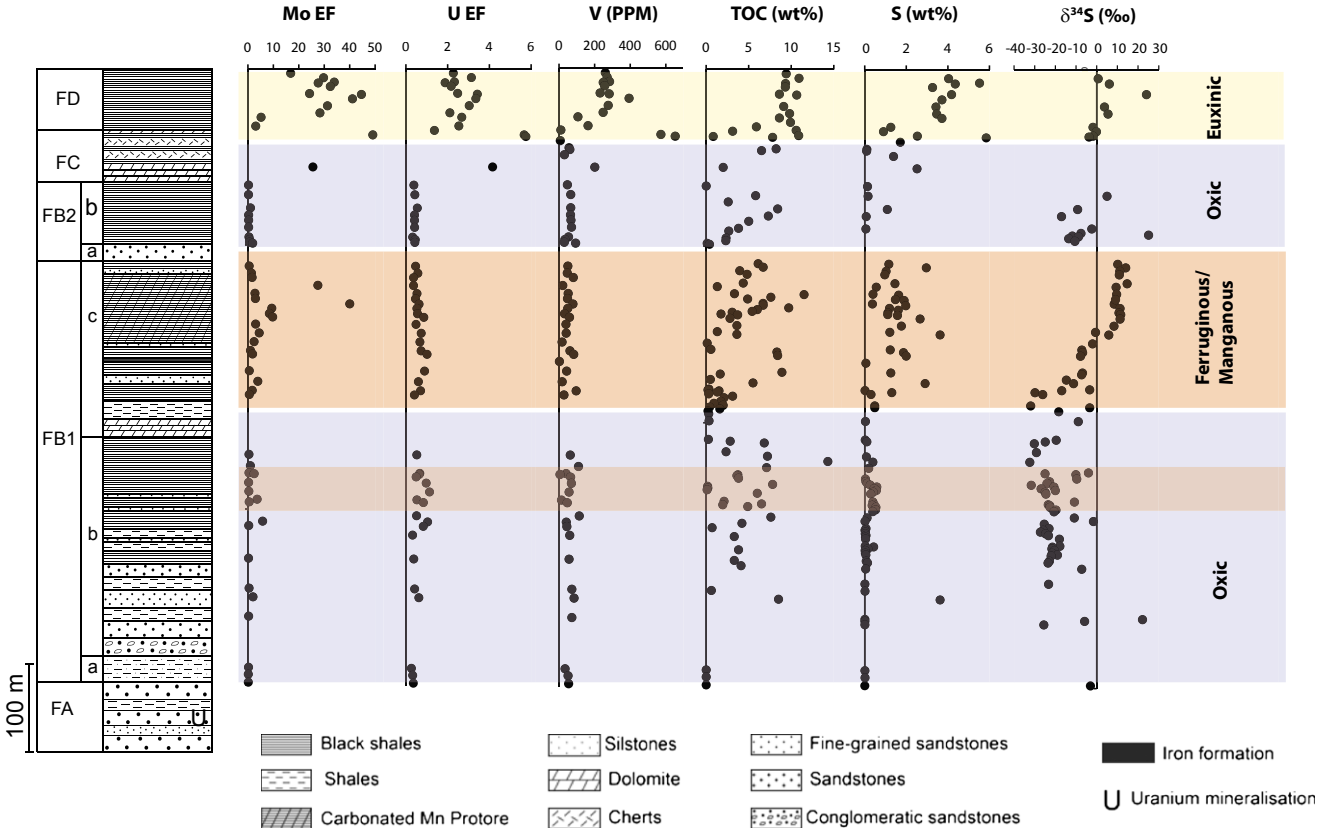

Fig. 2. Further trace metal and isotope data through the Francevillian sediments. Plotted also are metal enrichment factors (EF) for Mo and U. EF = $(X_{sediment}/Al_{sediment})/(X_{Crust}/Al_{Crust})$. X, metal content (wt%).

In evaluating our data, deposition under anoxic bottom water conditions is indicated if highly reactive Fe (FeHR) exceeds 38% of the total Fe (FeT) (37). If reactive Fe exceeds this amount, and if greater than 70–80% is pyrite (the amount of pyrite Fe is denoted FePy), deposition in a sulfide-rich euxinic environment is indicated, and, if less of the reactive Fe is pyritized, ferruginous water-column conditions are indicated (37–39). Oxic conditions are likely if reactive Fe is less than 38% of the total although this signal can also be generated under anoxic bottom-water conditions if, for example, sedimentation is particularly rapid. Therefore, comparisons with other geochemical indicators are useful in making final assessments about water-column redox chemistry as described below in this section.

Fe speciation results, together with a lack of trace-metal enrichment, indicate oxic deposition conditions through most of the relatively deep waters at the base of the FB1a subunit, with some indications for a transition to ferruginous conditions near the top of this subunit (Fig. 1). Oxic conditions were reestablished and continued to the base of the FB1c subunit. Anoxic ferruginous conditions developed through the following regression, switching to manganous conditions near the top of the FB1c subunit, with sediment Mn contents approaching 30 wt%. There is also the possibility of the intermittent establishment of euxinic conditions near the middle and top of the FB1c subunit as indicated by FeHR/FeT > 0.38 and FePy/FeT > 0.7 (without, however, accompanying enrichments in U and V, so euxinia, if established, was likely not severe) (Figs. 1 and 2). As regression continued, oxic conditions are revealed again in shallow sediments depositing in the boundary between the FB2 and FC units. Consistent with this evidence for oxygenated conditions, soft-bodied macroscopic fossils are found in the FB2b subunit (28), and stromatolites are found in dolomites and chert of the FC unit. We lack Fe speciation for the middle part of the FC, but we note enrichments in Mo, V, and U at a single depth in the middle of this unit (Figs. 1 and 2), and this trace metal enrichment could indicate fluctuating oxic/anoxic conditions in this interval. During subsequent transgression, Fe speciation and trace metal enrichments (Fig. 1) show the development of euxinic conditions at the top of the FC unit and into the deeper waters of the FD unit.

The FB1a and FB1b subunits were deposited in relatively deep water, and this oxygenation required sufficient atmospheric oxygen to ventilate the deep basin, providing, therefore, direct geochemical evidence for relatively high oxygen levels during the Lomagundi excursion. Other evidence for a well-oxygenated surface environment comes from highly $\delta^{34}S$-depleted sulfide values of −20‰ to −30‰ (Fig. 2). These isotope values yield fractionations during sulfate reduction of between 30‰ to 40‰, assuming a $\delta^{34}S$ of 10‰ for sulfate (24). Such high fractionations are consistent with an abundant sulfate pool of well over 200 μM in concentration (40), complimenting other evidence for elevated sulfate, including thick beds of evaporitic sulfate deposited during the Lomagundi excursion (17, 20, 22), as well as sulfate cements, layers, and other sulfate precipitates in various places in the FA and FC units in Gabon (21).

Mo Isotopes. The subsequent transition, however, to anoxic deep-water conditions in the FB1c subunit need not relate to fluctuations in atmospheric oxygen, but could equally have arisen from changes in basin geometry or basin circulation. For this reason, our evaluation of the Mo isotope signal is critical in establishing the global extent of deep water oxygenation through the final phases of the Lomagundi event and its aftermath. The Mo isotope system is particularly useful because Mo is well-mixed in the oceans and because its isotopic composition represents a balance between oxic and euxinic removal pathways. Oxic removal is onto Mn oxides, with a fractionation ($\delta^{98/95}Mo_{seawater\text{-}Mn\ oxide}$) of 3‰, and euxinic removal produces little or no fractionation (41) provided there is sufficient sulfide and time to convert molybdate to particle-reactive thiomolybdate forms (42, 43). It is well-established, however, that fractionations to depleted $\delta^{98/95}Mo$ values (compared with seawater) can occur when sulfide and or/time is limiting as in the upper reaches of the euxinic Black Sea (44). Thus, whereas ancient sediments deposited under demonstrably euxinic conditions are taken to capture the $\delta^{98/95}Mo$ of contemporaneous seawater, a spread of values may point to

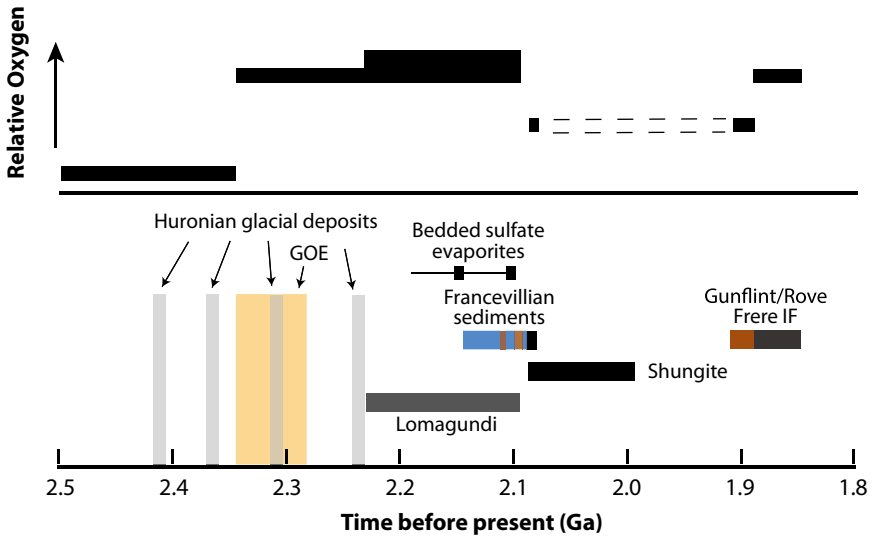

Fig. 3. (*Upper*) Reconstruction of relative trends in levels of oxygen based on information given in the text. Dotted line represents a time with little constraint as discussed in the text. (*Lower*) Outlines the timing of the depositional units used to reconstruct oxygen trends. Also shown are the depositional environment for the Francevillian sediments as shown in Fig. 1 as well as indications of intervals of massive bedded gypsum deposition as presented in refs. 20 and 55. The timing of the Huronian glaciations are after ref. 17, and the GOE after ref. 56. Uncertainties in the dating of the different deposits are represented in the length of the horizontal bars representing the various fields (see *Results and Discussion, Ocean and Atmospheric Oxygenation in the Wake of Lomagundi Excursion* for details). The chronology of the Francevillian sediments is discussed in the text. Note that the shungite deposits of Fennoscandia have been previously linked with deposition of the FD unit from Gabon (33).

nonquantitative removal from seawater. Therefore, the heaviest $\delta^{98/95}$Mo values are usually assumed to best reflect the seawater composition (45–47). In the modern oceans, the balance between oxic and anoxic removal pathways yields a seawater $\delta^{98/95}$Mo value of 2.3‰, the highest known in Earth history. Lower $\delta^{98/95}$Mo values will be expected with more euxinic removal down to values of between 0.4‰ to 0.7‰, representing the range between the crustal average (0.4‰) and modern river water input to the ocean (0.7‰,) (46, 48).

In Gabon, enrichments in Mo concentration are found in both of the well established anoxic intervals (Fig. 1). In the lower manganous interval, the $\delta^{98/95}$Mo values are curiously low, reaching down to −0.8‰ and falling well below both modern rivers and the crustal average. These fractionations, however, are completely consistent with removal through adsorption onto manganese oxides (41, 49), with ultimate capture into sediments underlying the manganous water column.

In the euxinic interval of the FD unit, values of $\delta^{98/95}$Mo range from 0.02‰ to 0.95‰, with an average of 0.3‰. Although this interval is clearly euxinic based on both the Fe extraction results and trace metal enrichments (Figs. 1 and 2), we cannot constrain the concentrations of sulfide in the basin. Therefore, we view the spread in isotope values, as is typical in ancient euxinic basins, to reflect variable removal of Mo into euxinic sediments and take the most enriched $\delta^{95/98}$Mo value of 0.95‰ as most representative of contemporaneous seawater. The alternative views are (*i*) that the cluster of lighter values are most representative of seawater and that the single heavy value represents some kind of local distillation effect, and (*ii*) that sulfide was sufficiently limiting throughout deposition of this whole section that the true seawater value was not captured and was heavier than the heaviest we report. These same issues plague all of the ancient Mo isotope record, and we feel a reasonable approach is to use our most enriched value as a reflection of contemporaneous seawater. If this value underestimates true seawater, it may still be reasonably compared with the rest of the ancient isotope record, which suffers from the same issue.

Taking this approach, even our most $\delta^{98/95}$Mo-enriched value of 0.95‰ is the most $\delta^{98/95}$Mo-depleted for any euxinic environment following the GOE (45–47) (Fig. S1). Indeed, the similarity of the $\delta^{98/95}$Mo values in the FD unit to the crustal average, and to modern riverine input, implies minimal removal of molybdenum from the oceans through oxic pathways. Therefore, our isotope data suggest that, during FD deposition, sulfidic marine conditions were as extensive as at any time during the Proterozoic Eon. The organic-rich "shungites" from the Fennoscandian of Russia (50) (*SI Text* and Table S1) likely also provide evidence for euxinic conditions at this time. As mentioned above, trends in the δ^{34}S of CAS sulfate through the Lomagundi excursion (24) are also consistent with increased euxinia through the later parts of the excursion, even though this dataset does not apparently extend to the time of FD deposition.

Ocean and Atmospheric Oxygenation in the Wake of the Lomagundi Excursion. From our results, the widespread marine euxinia during FD deposition represents a fundamentally different world than the extensive oxic conditions that persisted in deep waters of the Francevillian Basin while the Lomagundi event was in full force. The FD unit deposited in concert with a large negative shift in the δ^{13}C of both organic and inorganic carbon, likely signaling the weathering of the large amounts of organic carbon deposited during the Lomagundi event (33). The oxidation of this organic carbon would have represented a formidable oxygen sink, likely reducing the levels of atmospheric oxygen (24, 25), allowing, in turn, the widespread expansion of euxinic conditions as indicated by the geochemical record.

If we look toward younger rocks, we note that, by 1,890 Ma, banded iron formation (BIF) deposition became widespread, with conspicuous examples including the Frere Formation from Western Australia and various examples from the Superior Province in Canada, including the Gunflint Iron Formation (51). These BIFs are characterized by iron oxide precipitation in very shallow waters, requiring Fe^{2+} transport for long distances across the continental shelf. The oxidation rate of Fe^{2+} depends on oxygen availability, and Fe^{2+} could only have persisted in solution for cross-shelf transport under very low levels of atmospheric oxygen, estimated at about 0.1% of present levels (PAL; present atmospheric levels) (19, 52). Low atmospheric oxygen levels at this time would also be consistent with the Cr isotope record which shows no fractionation in the Gunflint BIF implying limited or no oxidative weathering of Cr from the continents (53).

Therefore, we have evidence for two episodes, within 200 million years of each other and well after the GOE, where atmospheric oxygen was reduced to levels well below those reached during the GOE and the Lomagundi excursion. At around 1,900 Ma, a pulse of Fe^{2+} from increased mantle activity could have contributed to the Fe^{2+} depositing in the Gunflint and other time-equivalent BIFs, and an associated increase in the flux of reduced gases could have generated an enhanced sink for atmospheric oxygen (51). However, as explored above, the geochemical record also indicates a reduction in oxygen levels during the deposition of FD formation in Gabon, some 200 million years before this time. The intervening geochemical record is poor, but we entertain the possibility that these two episodes of low-oxygen conditions are linked. In this scenario, the oxidation during weathering of elevated levels of organic carbon deposited during the Lomagundi excursion provided a drain on atmospheric oxygen lasting for some 200 million years after the end of the excursion (Fig. 3). Such a time scale would be consistent with the recycling time of crustal rocks to weathering (54). As the Lomagundi organic carbon became oxidized away, oxygen rose again to values typical of the middle Proterozoic Eon. This rise in oxygen is indicated by the reappearance at 1,840 Ma of fractionated Cr, together with $\delta^{98/95}$Mo values of up to 1.4‰ (47), which are considerably enriched compared with values from unit FD in Gabon. In another scenario, atmospheric oxygen levels exhibited dynamic behavior after the Lomagundi event, with at least two excursions to low values, the first as captured in the FD unit and the second as reflected in the Gunflint and associated iron formations.

We cannot at present distinguish between these two possibilities for the history of atmospheric oxygen. Regardless of which is correct, the accumulated evidence suggests that the aftermath of the GOE saw massive swings in the levels of atmospheric oxygen. It is also possible, as explored here, that these swings were indirectly a result of the GOE itself. In this scenario, which is consistent with the available evidence, the liberation of nutrients during oxidative weathering associated with the GOE increased the productivity of the oceans, likely elevating oxygen beyond GOE levels, producing the Lomagundi isotope event. As the source of nutrients from continental weathering waned, so did the Lomagundi event. Its organic matter, when brought into the weathering environment, caused a long-lasting drain on oxygen levels that subsided only after Lomagundi carbon became oxidized away.

ACKNOWLEDGMENTS. We thank the Gabon Ministry of Education and Research, Centre National de la Recherche Scientifique, the Gabon Ministry of Mines, Oil, Energy and Hydraulic Resources, the General Direction of Mines and Geology, the Sylvia Bongo Ondimba Foundation, Agence Nationale des Parcs Nationaux of Gabon, the COMILOG and SOCOBA Companies, and the French Embassy at Libreville for collaboration and technical support. For assistance, we thank B. Goffe, R. Macchiarelli, P. Mouguiama, J. C. Balloche, F. Pambo, A. Texier, L. White, and F. Weber. We thank the Danish National Research Foundation (Grant DNRF53), the European Research Council, Centre National de la Recherche Scientifique, Institut National des Sciences de l'Univers, Institut National de Chimie, Fond Européen pour le Développement Régional, the University of Poitiers, and the Région Poitou-Charente for financial support.

1. Holland HD (1994) Early Proterozoic atmospheric change. *Early Life on Earth*, ed Bengston S (Columbia Univ Press, New York), pp 237–244.
2. Rye R, Holland HD (1998) Paleosols and the evolution of atmospheric oxygen: A critical review. *Am J Sci* 298(8):621–672.
3. Farquhar J, Bao HM, Thiemens M (2000) Atmospheric influence of Earth's earliest sulfur cycle. *Science* 289(5480):756–759.
4. Holland HD (1999) When did the Earth's atmosphere become oxic? A reply. *Geochem News* 100:20–22.
5. Kirschvink JL, Kopp RE (2008) Palaeoproterozoic ice houses and the evolution of oxygen-mediating enzymes: The case for a late origin of photosystem II. *Philos Trans R Soc Lond B Biol Sci* 363(1504):2755–2765.
6. Catling DC, Zahnle KJ, McKay CP (2001) Biogenic methane, hydrogen escape, and the irreversible oxidation of early Earth. *Science* 293(5531):839–843.
7. Kasting JF, Eggler DH, Raeburn SP (1993) Mantle redox evolution and the oxidation state of the Archean atmosphere. *J Geol* 101(2):245–257.
8. Kump LR, Kasting JF, Barley ME (2001) Rise of atmospheric oxygen and the "upside-down" archean mantle. *Geochem Geophys Geosyst* 2:2000GC000114.
9. Holland HD (2009) Why the atmosphere became oxygenated: A proposal. *Geochim Cosmochim Acta* 73(18):5241–5255.
10. Melezhik VA, et al. (2013) The paleoproterozoic perturbation of the global carbon cycle: The Lomagundi-Jatuli isotopic event. *Reading the Archive of Earth's Oxgenation*, eds Melezhik VA, Kump LR, Strauss H, Hanski EJ, Prave AR (Springer, Heidelberg), Vol 3, pp 1111–1150.
11. Karhu JA, Holland HD (1996) Carbon isotopes and the rise of atmospheric oxygen. *Geology* 24:867–870.
12. Maheshwari A, et al. (2010) Global nature of the Paleoproterozoic Lomagundi carbon isotope excursion: A review of occurrences in Brazil, India, and Uruguay. *Precambrian Res* 182(4):274–299.
13. Schidlowski M, Eichmann R, Junge CE (1976) Carbon isotope geochemistry of the Precambrian Lomagundi carbonate province, Rhodesia. *Geochim Cosmochim Acta* 40(4):449–455.
14. Martin AP, et al. (2013) Dating the termination of the Palaeoproterozoic Lomagundi-Jatuli carbon isotopic event in the North Transfennoscandian Greenstone Belt. *Precambrian Res* 224:160–168.
15. Kump LR, Garrels RM (1986) Modeling atmospheric O_2 in the global sedimentary redox cycle. *Am J Sci* 286:337–360.
16. Berner RA (2004) *The Phanerozoic Carbon Cycle: CO_2 and O_2* (Oxford Univ Press, Oxford).
17. Bekker A, Holland HD (2012) Oxygen overshoot and recovery during the early Paleoproterozoic. *Earth Planet Sci Lett* 317–318:295–304.
18. Holland HD (2002) Volcanic gases, black smokers, and the great oxidation event. *Geochim Cosmochim Acta* 66(21):3811–3826.
19. Canfield DE (2005) The early history of atmospheric oxygen: Homage to Robert M. Garrels. *Annu Rev Earth Planet Sci* 33:1–36.
20. Schroeder S, Bekker A, Beukes NJ, Strauss H, van Niekerk HS (2008) Rise in seawater sulphate concentration associated with the Paleoproterozoic positive carbon isotope excursion: Evidence from sulphate evaporites in the similar to 2.2-2.1 Gyr shallow-marine Lucknow Formation, South Africa. *Terra Nova* 20(2):108–117.
21. Préat A, et al. (2011) Paleoproterozoic high $\delta^{13}C$ dolomites from the Lastoursville and Franceville basins (SE Gabon): Stratigraphic and synsedimentary subsidence implications. *Precambrian Res* 189(1-2):212–228.
22. Strauss H, et al. (2013) Abundant marine calcium sulphates: Radical changes of seawater sulphate reservoir and sulphur cycle. *Reading the Archive of Earth's Oxygenation*, eds Melezhik VA, et al. (Springer, Heidelberg), Vol 3, pp 1169–1194.
23. Partin CA, et al. (2013) Large-scale fluctuations in Precambrian atmospheric and oceanic oxygen levels from the record of U in shales. *Earth Planet Sci Lett* 369-370: 284–293.
24. Planavsky NJ, Bekker A, Hofmann A, Owens JD, Lyons TW (2012) Sulfur record of rising and falling marine oxygen and sulfate levels during the Lomagundi event. *Proc Natl Acad Sci USA* 109(45):18300–18305.
25. Canfield DE, Proterozoic atmospheric oxygen. *Treatise on Geochemistry*, ed Farquhar J (Springer, Amsterdam), Vol 13.
26. Weber F (1968) *Une série précambrienne du Gabon: le Francevillien. Sédimentologie, Géochimie, realtions avec les gites minéraux associés* (Alsace-Lorraine, Strasbourg, France).
27. Gauthier-lafaye F, Weber F, Ohmoto H (1989) Natural fission reactors of Oklo. *Econ Geol* 84(8):2286–2295.
28. El Albani A, et al. (2010) Large colonial organisms with coordinated growth in oxygenated environments 2.1 Gyr ago. *Nature* 466(7302):100–104.
29. Bertrand-Sarfati J, Potin B (1994) Microfossiliferous cherty stromatolites in the 2000 Ma Fanceville Group, Gabon. *Precambrian Res* 65(1-4):341–356.
30. Bros R, Stille P, Gauthier-Lafaye F, Weber F, Clauer N (1992) Sm-Nd isotopic dating of Proterozoic clay material- and example from the Francevillian sedimentary series, Gabon. *Earth Planet Sci Lett* 113(1-2):207–218.
31. Horie K, Hidaka H, Gauthier-LaFaye F (2005) U-Pb geochronology and geochemistry of zircon from the Franceville series at Bidoudouma, Gabon. *Geochim Cosmochim Acta* 69(10):A11.
32. Bonhomme MG, Gauthier-Lafaye F, Weber F (1982) An example of lower proterozoic sediments: The francevillian in Gabon. *Precambrian Res* 18:87–102.
33. Kump LR, et al. (2011) Isotopic evidence for massive oxidation of organic matter following the great oxidation event. *Science* 334(6063):1694–1696.
34. Gauthier-Lafaye F, Weber F (2003) Natural nuclear fission reactors: Time constraints for occurrence, and their relation to uranium and manganese deposits and to the evolution of the atmosphere. *Precambrian Res* 120(1-2):81–100.
35. Strauss H, et al. (2013) Enhanced accumulation of organic matter: The Shunga event. *Reading the Archive of Earth's Oxygenation*, eds Melezhik VA, et al. (Springer, Heidelberg), Vol 3, pp 1195–1273.
36. Weber F, Gauthier-Lafaye F (2013) No proof from carbon isotopes in the Francevillian (Gabon) and Onega (Fennoscandian shield) basins of a global oxidation event at 1980-2090 Ma following the Great Oxidation Event (GOE). *C R Geosci* 345(1):28–35.
37. Raiswell R, Canfield DE (1998) Sources of iron for pyrite formation in marine sediments. *Am J Sci* 298:219–245.
38. Poulton SW, Krom MD, Raiswell R (2004) A revised scheme for the reactivity of iron (oxyhydr)oxide minerals towards dissolved sulfide. *Geochim Cosmochim Acta* 68(18): 3703–3715.
39. Raiswell R, Canfield DE (2012) The iron biogeochemical cycle past and present. *Geochem Perspect* 1(1):1–220.
40. Habicht KS, Gade M, Thamdrup B, Berg P, Canfield DE (2002) Calibration of sulfate levels in the archean ocean. *Science* 298(5602):2372–2374.
41. Arnold GL, Anbar AD, Barling J, Lyons TW (2004) Molybdenum isotope evidence for widespread anoxia in mid-Proterozoic oceans. *Science* 304(5667):87–90.
42. Erickson BE, Helz GR (2000) Molybdenum(VI) speciation in sulfidic waters: Stability and lability of thiomolybdates. *Geochim Cosmochim Acta* 64(7):1149–1158.
43. Dahl TW, et al. (2010) The behavior of molybdenum and its isotopes across the chemocline and the sediments od sulfidic Lake Gadagno, Switzerland. *Geochim Cosmochim Acta* 74:144–163.
44. Nagler TF, Neubert N, Bottcher ME, Dellwig O, Schnetger B (2011) Molybdenum isotope fractionation in pelagic euxinia: Evidence from the modern Black and Baltic Seas. *Chem Geol* 289(1-2):1–11.
45. Dahl TW, et al. (2010) Devonian rise in atmospheric oxygen correlated to the radiations of terrestrial plants and large predatory fish. *Proc Natl Acad Sci USA* 107(42): 17911–17915.
46. Dahl TW, et al. (2011) Molybdenum evidence for expansive sulfidic water masses in ~750 Ma oceans. *Earth Planet Sci Lett* 311(3–4):264–274.
47. Kendall B, Gordon GW, Poulton SW, Anbar AD (2011) Molybdenum isotope constraints on the extent of late Paleoproterozoic ocean euxinia. *Earth Planet Sci Lett* 307(3-4):450–460.
48. Archer C, Vance D (2008) The isotopic signature of the global riverine molybdenum flux and anoxia in the ancient oceans. *Nat Geosci* 1(9):597–600.
49. Siebert C, Nagler TF, von Blanckenburg F, Kramers JD (2003) Molybdenum isotope records as a potential new proxy for paleoceanography. *Earth Planet Sci Lett* 211(1-2): 159–171.
50. Melezhik VA, Fallick AE, Filippov MM, Larsen O (1999) Karelian shungite-an indication of 2.0-Ga-old metamorphosed oil-slae and generation of petroleum: Geology, lithology and geochemistry. *Earth Sci Rev* 47:1–40.
51. Rasmussen B, et al. (2012) Deposition of 1.88-billion-year-old iron formations as a consequence of rapid crustal growth. *Nature* 484(7395):498–501.
52. Holland HD (2003) The geological history of seawater. *Treatise on Geochemistry*, eds Holland HD, Turekian KK (Elsevier, Oxford), Vol 6, pp 583–625.
53. Frei R, Gaucher C, Poulton SW, Canfield DE (2009) Fluctuations in Precambrian atmospheric oxygenation recorded by chromium isotopes. *Nature* 461(7261):250–253.
54. Garrels RM, Mackenzie FT (1971) *Evolution of Sedimentary Rocks* (Norton, New York).
55. Reuschel M, et al. (2012) Isotopic evidence for a sizeable seawater sulfate reservoir at 2.1 Ga. *Precambrian Res* 192-95:78–88.
56. Guo Q, et al. (2009) Reconstructing Earth's surface oxidation across the Archean-Proterozoic transition. *Geology* 37:399–402.

Supporting Information

Canfield et al. 10.1073/pnas.1315570110

SI Text

Sample Collection, Trace Metal Analysis, and Iron Speciation

Samples were collected from both outcrop and drill core material, with similar results in overlapping strata. Iron speciation analyses followed ref. 1 whereas sulfur (relative to Cañon Diablo troilite) and carbon (relative to PDB) isotope analyses were performed by isotope ratio mass spectrometry (Thermo Delta plus) following combustion in an elemental analyzer. Trace metals were determined after first powdering rock samples (300 mg) and then fusion along with 900 mg of ultra-pure $LiBO_2$ at 980 °C in an automatic tunnel oven. Samples were passed through the oven on a rail over a period of about 60 min at a constant speed, ensuring that all of the samples encountered the same thermal gradient. After cooling to room temperature, the fusion glass was dissolved in an HNO_3 (1 mol/L)-H_2O_2 (0.5%)-glycerol (10%, vol/vol) mixture to a dilution factor of 333 relative to the amount of sample fused. Trace metals were measured by inductively coupled plasma mass spectrometry (ICP-MS) (Thermo ×7) using a one point "linear through zero" calibration whereas major elements were determined by inductively coupled plasma-optical emission spectrometry (ICP OES) (Thermo Icap 6500). Organic carbon concentrations were determined after acid treatment to remove carbonate using a Leco SC144 DR whereas sulfur contents were determined by either weighing Ag_2S precipitates after Cr distillation of the samples to liberate reduced sulfur (2), or directly with the Leco SC144 DR. Molybdenum isotopes were determined by multi-collector plasma-optical emission spectrometry (MC-ICP-MS), with a full description in *Mo-Isotope Analyses*. Relative sea level trends were determined by lithofacies study on the whole Francevillian group based on direct observations of outcrops and cores.

Mo-Isotope Analyses

Due to the high content of organic matter, all samples were ashed in quartz beakers at 600 °C for at least 24 h. All later chemical procedures were undertaken in clean laboratories, using distilled acid (HNO_3; HCl) or trace metal grade HF. About 200 mg of ashed sample was dissolved in concentrated HNO_3 (7 mL) + HF (1.5 mL) and evaporated on a hot plate at 60 °C. Dry residues were further dissolved with concentrated HNO_3 + HCl, taken to dryness, and finally redissolved with 20 mL of 7N HCl. Depending on the Mo concentration, a portion of each sample solution was doped with Mo double spike to keep a constant spike/sample ratio, and the samples were then subject to chromatographic separation as described in refs. 3 and 4. Briefly, Mo purification was done in a two-stage column procedure: in the first stage, an anion resin separated Mo (Biorad AG-MP1) and most of the Fe from the matrix, and in a second stage, a cation resin separated Mo from the remaining Fe (Biorad AG-50 × 8). Mo isotope composition measurements were done using a Thermo Neptune MC-ICP-MS instrument at the Pole Spectrometrie Ocean, Brest at IFREMER (France).

We used ^{97}Mo-^{100}Mo double-spike solution prepared gravimetrically from Oak Ridge Laboratory metal powders. Optimization of the double-spike isotope composition relative to the SPEX standard gave ^{95}Mo/^{98}Mo, ^{97}Mo/^{98}Mo, and ^{100}Mo/^{98}Mo isotopic ratios of 0.278, 16.663, and 15.704, respectively. Data reduction was done according to ref. 5 where iterations were repeating while the difference in the δ^{98}Mo value between two consecutive iterations was smaller than 0.001‰. The typical number of iterations was ≤4. Molybdenum concentrations varied from 100 to 500 parts per billion (ppb), depending on the Mo content of the sample powders. Within each session, standards and samples were measured at a constant concentration. The external precision of the measurement was $2\sigma = \pm 0.04$‰ whereas the typical SE of a single measurement was $2\sigma = 0.05$‰. Molybdenum concentrations were derived from the spike/sample ratio determined as part of the double-spike data reduction scheme. The MC-ICP-MS machine was operated at low resolution with an ESI Apex Q introduction system measuring all Mo isotope masses together with ^{91}Zr and ^{99}Ru to monitor isobaric interferences.

During each session of Mo-isotope measurements, we performed frequent measurements of our in-house laboratory Mo standard (Mo SPEX lot 11–177Mo), measurements of the NIST-3137 standard, and the Johnson Matthey Specpure Mo plasma standards (Lot no. 802309E; RochMo2) used in previous studies (3). We also preformed frequent measurements of geo-reference materials including SDO-1, Nod A-1, and Nod P-1.

Molybdenum isotopic compositions are all reported here using the δ notation (in terms of ^{98}Mo/^{95}Mo ratios) calculated relative to our in-laboratory Mo SPEX standard (lot 11–177Mo). A calibration of the SPEX standard relative to NIST-3137 (lot 891307) and Rochester (lot 802309E) standards (supplied by the laboratory of A. D. Anbar, Arizona State University) gave:

$$\delta^{98/95}\mathrm{Mo_{SPEX}} = \delta^{98/95}\mathrm{Mo_{NIST3137}} - 0.35 \pm 0.06‰$$
$$\delta^{98/95}\mathrm{Mo_{SPEX}} = \delta^{98/95}\mathrm{Mo_{Mo\text{-}Roch}} - 0.05 \pm 0.03‰.$$

We choose to report our results relative to the SPEX standard because, within error, it is identical to the Rochester standard, which is the most common standard in recent Mo-isotope literature.

Shungite Depositional Environment

The most comprehensive description of shungite chemistry comes from the study of ref. 6. The distribution of C/S ratios from these sediments falls within the range of nonmarine fresh-water sediments, leading the authors to conclude that "the sediments deposited in swampy, brackish water lagoon under noneuxinic condition." However, the shungites are not well-suited to environmental interpretations based on C/S ratios because the shungites are extremely rich in organic carbon, approaching 100% in some cases, and very poor in Fe (Table S1). Thus, there is insufficient Fe to capture the sulfide produced by sulfate reduction, making the C/S ratio of little use in environmental interpretations (Table S1). The shungites, however, are rich in Mo and V, to the same level as the euxinic Francevillian sediments and thus are completely consistent with deposition in a euxinic environment. The shungites also have high ratios of pyrite Fe (FePy)/total Fe (FeT). In many cases, it appears that all or nearly all of the Fe is completely pyritized. In other cases, some of the Fe is clearly not pyritized, but anoxic sediments deposited in euxinic environments can have FePy/FeT ratios between about 0.3 and 1.0 [the low end is with highly reactive Fe (FeHR)/FeT of 0.4 and FePy/FeHR of 0.7 whereas, in the upper end, both of these ratios are 1]. A direct comparison with modern depositional environment would be possible if highly reactive Fe contents were available, but they unfortunately are not.

1. Poulton SW, Canfield DE (2005) Development of a sequential extraction procedure for iron: Implications for iron partitioning in continentally-derived particulates. *Chem Geol* 214:209–221.

2. Canfield DE, Raiswell R, Westrich JT, Reaves CM, Berner RA (1986) The use of chromium reduction in the analysis of reduced inorganic sulfur in sediments and shales. *Chem Geol* 54:149–155.

3. Barling J, Arnold GL, Anbar AD (2001) Natural mass-dependent variations in the isotopic composition of molybdenum. *Earth Planet Sci Lett* 193(3-4):447–457.
4. Wille M, et al. (2007) Evidence for a gradual rise of oxygen between 2.6 and 2.5 Ga from Mo isotopes and Re-PGE signatures in shales. *Geochim Cosmochim Acta* 71(10): 2417–2435.
5. Siebert C, Nagler TF, Kramers JD (2001) Determination of molybdenum isotope fractionation by double-spike multicollector inductively coupled plasma mass spectrometry. *Geochem Geophys Geosyst* 2:2000GC000124.
6. Melezhik VA, Fallick AE, Filippov MM, Larsen O (1999) Karelian shungite-an indication of 2.0-Ga-old metamorphosed oil-slae and generation of petroleum: Geology, lithology and geochemistry. *Earth Sci Rev* 47:1–40.

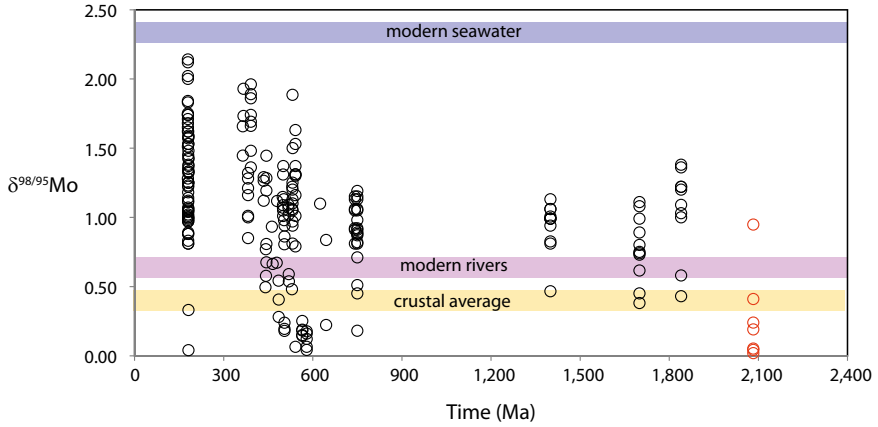

Fig. S1. The isotopic composition of Mo ($\delta^{98/95}$Mo) since the GOE. Data from Gabon are shown in red. Other data are from the compilation presented in ref. 1; original references can be found there.

1. Raiswell R, Canfield DE (2012) The iron biogeochemical cycle past and present. *Geochem Perspect* 1(1):1–220.

Table S1. Data for *ca.* 2.1 Ga Fennoscandian shungites (from ref. 6)

Sample	TOC	S, wt%	Fe, wt%	FePy/FeT	Mo, ppm	Mo/TOC	V, ppm
1	2.0	B.D.	0.10		41	20.5	59
2	37.7	0.1	0.17	0.52	7	0.18	117
3	35.5	B.D.	0.11		10	0.28	127
4	31.4	0.4	1.07	0.32	12	0.38	154
5	N.D.	0.5	0.61	0.72	49		416
6	N.D.	2.2	1.41	1.37	38		483
7	1.0	B.D.	0.10		7	7.0	46
8	1.4	B.D.	0.08		8	5.71	78
9	64.1	5.0	7.66	0.57	237	3.70	1,304
10	56.7	3.8	6.72	0.49	258	4.55	1,667
11	98.4	0.2	N.D		168	1.71	940
12	90.0	0.6	0.13	4.16	B.D.		54
13	0.9	B.D.	9.67		B.D.		227
14	25.2	B.D.	0.87		40	1.59	589
15	45.5	B.D.	0.18		86	1.89	593

B.D., below detection; Ga, billion years ago; N.D., not determined; ppm, parts per million; TOC, total organic carbon.

Table S2. Data from Francevillian samples of the current study

Formations	Mo,ppm	U, ppm	Fe, wt%	Al, wt%	Mn, wt%	V, ppm	FeHR/FeT	FePy/FeHR	S, wt%	$\delta^{34}S$	TOC, wt%	$\delta^{13}Corg$	$\delta^{98/95}Mo$
	22.18	6.01	0.00	6.97	0.01	259.60					9.40	−46.00	0.02
	31.91	6.73	5.30	5.65	0.03	270.00	0.76	0.90	4.03	0.64	10.90	−45.98	0.05
	39.70	5.43	6.25	6.17	0.05	283.30			5.52				
	34.40	4.68	5.71	6.56	0.08	247.90	0.75	0.90	4.35	6.07	9.32	−45.68	0.04
	40.20	5.38	4.29	6.54	0.09	256.00	0.49	0.79	3.26		9.30	−45.70	
FD	28.04	5.74	5.77	6.10	0.22	230.60	0.69	0.87	4.17	23.99	8.60	−45.20	0.41
	43.20	6.63	6.41	5.10	0.02	281.60	0.90	0.87	6.02		10.64	−45.22	
	41.30	6.73	4.54	5.29	0.06	393.20			3.71				
	31.69	6.15	4.48	5.34	0.01	275.90	0.65	0.80	3.42	3.69	9.10	−46.10	0.19
	30.41	4.52	4.94	5.66	0.05	247.40	0.81	0.61	3.46	5.43	9.80	−46.20	0.24
	5.28	5.48	5.92	5.39	0.15	105.60	0.81	0.69	3.71		8.60	−48.00	0.95
											9.90	−46.20	
	2.65	4.40	4.01	4.58	0.13	162.60	0.44	0.53	1.25	−1.84	5.90	−46.30	
			0.00	0.00							10.57	−40.40	
	< L.D	0.99	1.93	1.91	1.14	10.00	0.46	0.61	0.90	−0.21	3.10	−43.30	
	27.00	6.23	2.39	2.90	0.01	571.90	0.93	0.89	2.53	−1.82	10.87	−31.98	
							0.93	0.85		−3.77	0.82	−41.17	
	64.80	7.83	5.35	3.59	0.04	652.20	0.83	0.72	5.84		7.80	−38.80	
	3.59	1.82	1.60	0.29	0.01	7.10			1.71				
FC	1.47	1.52	0.28	7.06	0.00	56.12	0.18	0.25	0.10		8.22	−35.12	
	1.42	1.53	0.28	7.47	0.00	60.20	0.27	0.27	0.09		6.51	−35.09	
	1.31	1.25	1.48	0.79	0.03	30.10			1.38				
											2.00	−37.10	
	10.65	3.47	2.37	2.29	0.01	200.30			2.51				
	0.33	1.22	0.88	8.46	0.02	46.55			0.13		—	—	
	0.47	1.73	1.34	10.74	0.02	65.63	0.17	0.51	0.16	4.95	5.80	−32.60	
											2.59	−32.46	
	1.67	1.88	1.85	9.09	0.04	65.32	0.65	0.65	1.08	−9.30	8.40	−32.95	
	0.51	1.62	2.28	10.50	0.15	63.87	0.26	0.29	0.07	−17.10	7.30	−32.50	
	0.51	1.58	2.81	10.14	0.14	66.66					5.00	−32.40	
	0.50	1.54	3.33	9.77	0.13	69.45	0.08	0.27	0.05	−2.42	3.80	−33.46	
											2.65	−33.55	
FB2b							0.14	0.32		−7.70			
							0.33	0.04		25.00			
							0.27	0.14		−11.87			
							0.37	0.24		−8.88			
	0.76	1.21	2.41	9.87	0.05	52.97	0.35	0.13		−13.59	2.33	−35.10	
	0.76	1.08	4.54	6.38	0.57	32.39	0.14	0.37		−10.60	2.30	−34.60	
	0.72	1.02	6.20	6.37	0.08	29.13					0.12	−32.70	
	2.92	1.00	0.29	8.28	0.00	92.65					0.39	−30.15	
							0.90	0.62	1.16	10.14	6.10	−34.11	
	0.58	1.16	2.80	6.63	0.06	49.35	0.78	0.61	2.96	13.98	6.70	−35.00	0.30
							1.10	0.78	1.03	11.07	3.93	−35.11	
	1.15	0.95	0.94	4.37	1.46	46.10	1.13	0.82	0.96	10.88	4.80	−33.80	
	1.82	0.80	2.09	5.81	5.41	80.00						−34.60	
							1.19	0.72	1.45	14.65	4.35	−34.16	
	7.05	0.19	0.50	1.35	13.89	20.45	0.91	0.55	0.55	9.30	1.30	−33.60	−0.74
			2.12	3.48	11.75		0.80	0.28	0.40	9.58	3.32	−33.77	
	2.75	1.07	2.49	5.29	13.65	50.81			1.63		11.50	−34.49	
			1.87	3.70	13.19		0.93	0.33	0.37	8.43	6.68	−33.58	
			1.76	3.64	9.23						7.60	−33.70	
			2.18	7.57	6.13		0.84	0.58	1.47	9.06	4.87	−34.07	
	3.57	1.11	2.01	6.46	0.09	47.24			1.89				
	24.77	0.78	1.88	3.26	19.63	77.59			1.97		6.70	−34.02	
			1.88	4.55	0.83		1.17	0.65	1.19	11.23	9.70	−34.00	
	5.57	0.62	1.52	3.14	16.14	48.54			1.61		6.00	−33.86	−0.59
			1.23	2.43	14.16						5.40	−33.30	
			1.38	2.23	14.60		1.17	0.64	1.11	10.71	3.05	−32.69	
			1.38	2.12	15.67		1.17	0.64	1.11	11.57	1.74	−32.39	
	3.48	0.46	1.56	2.18	21.15	30.65	0.90	0.50	1.57		3.70	−33.12	

Table S2. Cont.

Formations	Mo,ppm	U, ppm	Fe, wt%	Al, wt%	Mn, wt%	V, ppm	FeHR/FeT	FePy/FeHR	S, wt%	$\delta^{34}S$	TOC, wt%	$\delta^{13}Corg$	$\delta^{98/95}Mo$
	7.09	1.25	2.47	3.85	9.78	58.51	0.98	0.55	2.66	11.26	2.80	−33.20	−0.16
	1.33	0.42	1.79	2.31	16.84	38.50	0.92	0.73	1.76	8.32	3.60	−32.40	
							0.78	0.25	1.20	−0.64	1.30	−32.31	
FB1c	3.03	1.00	3.12	3.60	16.19	39.57	0.66	0.48	3.62	5.80	3.60	−31.30	
	0.63	0.35	6.75	1.38	17.16	16.76	0.64	0.34		−2.09	0.12	−31.36	−0.25
							0.76	0.34	1.22	−7.27	0.55	−30.89	
	1.00	1.49	1.82	5.41	0.17	60.74	1.04	0.90	1.86	−6.88	8.30	−30.20	
	2.31	2.61	2.05	6.80	0.06	82.52	1.08	0.85	1.99	−7.91	8.40	−30.10	
	2.57		35.91	0.09	0.49	2.05			0.05				
	0.59	2.03	1.78	6.01	0.09	42.08	0.21	0.79	1.25	−6.93	8.90	−28.80	
							0.78	0.79		−7.37	1.65	−29.48	
							0.69	0.56		−14.74	0.49	−29.99	
	3.07	0.95	3.07	4.20	0.10	17.42	1.02	0.90	2.90	−11.28	5.50	−27.80	
							0.37	0.02		−3.47	0.32		
							0.54	0.01	0.01	−16.97	0.20	−28.71	
											1.50	−27.42	
	1.67	1.39	3.80	5.23	0.05	95.80	0.52	0.64	1.30	−29.89	1.30	−27.06	
							0.67	0.23	0.30	−26.17	0.30		
	0.64	1.01	1.79	6.60	0.01	27.57					3.10	−26.78	
											2.10	−27.17	
											1.70	−27.65	
											0.90	−26.51	
							0.71	0.39	0.48	−31.97	2.00	−27.47	
							0.37	0.02	0.48	−3.47	0.40	−26.91	
							0.17	0.10			1.60	−26.90	
							0.31	0.10		−18.41	0.20	−26.52	
											0.30	−26.49	
			3.11	7.41			0.17	0.10	0.03	−8.94	0.33	−28.19	
							0.11	0.08	0.02	−19.65	0.26	−26.61	
			3.11	10.06			0.16	0.39	0.10	−24.96	2.82	−26.37	
							0.28	0.29		−30.25	6.82	−24.54	
							0.37	0.36		−29.20	2.33	−24.37	
	0.73	2.03	5.43	10.34	0.07	62.89	0.12	0.12	0.08		7.20	−24.50	1.31
							0.35	0.44	0.39	−32.41	14.29	−21.91	
	1.71	116.60	1.07	9.52	0.00	108.90			0.19		7.10	−22.90	
							0.36	0.34		−4.05			
							0.52	0.69		−25.07			
							0.17	0.36		−10.11			
	0.49	1.60	3.09	6.35	0.27	39.22					3.72		
	0.38	0.20	1.08	0.83	0.18	5.08					3.60	−23.92	
	< L.D	1.74	2.43	9.41	0.31	65.03	0.07	0.06	0.03	−9.71	3.80	−24.16	
							0.12	0.20	0.05	−22.84			
							0.31	0.20	0.12	−24.15			
	0.42	3.26	2.17	8.85	0.35	69.40	0.43	0.42	0.27	−31.74	7.80	−24.11	
							0.43	0.48	0.58	−20.73	0.17	−24.46	
							0.42	0.47	0.45	−26.95	0.19	−26.08	
							0.46	0.48	0.56	−20.06	0.11	−25.55	
							0.36	0.40	0.40	−24.96		−25.10	
	0.54	3.36	3.12	7.84	0.41	56.20	0.36	0.28	0.28	−24.60	6.00	−23.90	−1.10
	1.55	0.45	8.60	2.26	0.85	14.00	0.57	0.01	0.39	−10.81	2.10	−23.70	−0.30
FB1b	0.75	2.58	2.47	8.15	0.20	46.02	0.40	0.37	0.45	−23.47	6.50	−23.42	−0.09
							0.36	0.36	0.35	−22.74	1.94	−25.06	
							0.37	0.58	0.54	−22.59	4.88	−24.32	
							0.30	0.49	0.51	−19.77			
							0.30	0.53	0.38	−20.71			
	0.33	2.31	1.32	12.01	0.02	113.30	0.22	0.17	0.11	−10.87	7.60	−24.44	
							0.13	0.04	0.01	−1.62			
	2.37	0.85	22.99	2.17	0.60	40.78	0.48	0.20	21.00	−25.44	4.20	−24.50	
	0.42	2.46	6.41	7.81	0.02	43.62	0.17	0.11	0.06	−23.11	0.70	−23.68	
							0.08	0.08	0.01	−25.99			
							0.09	0.15	0.03	−27.28			

Table S2. Cont.

Formations	Mo,ppm	U, ppm	Fe, wt%	Al, wt%	Mn, wt%	V, ppm	FeHR/FeT	FePy/FeHR	S, wt%	$\delta^{34}S$	TOC, wt%	$\delta^{13}Corg$	$\delta^{98/95}Mo$
							0.06	0.15	0.02	−24.71			
							0.07	0.08	0.06	−23.39			
	< L.D	1.32	1.81	11.02	0.00	59.51	0.14	0.10	0.03		3.30	−24.65	
							0.17	0.10	0.04	−18.09			
							0.09	0.09	0.02	−17.86			
							0.24	0.46	0.43	−21.44			
							0.17	0.37	0.15	−21.73			
									0.02	−20.58	3.80	−23.95	
							0.09	0.04	0.02	−21.55			
							0.09	0.12	0.05	−19.04			
							0.16	0.08		−22.11			
	0.44	1.52	2.50	10.74	0.02	56.01	0.20	0.18	0.07	−22.94	3.30	−30.01	
							0.16	0.34	0.13	−23.61			
											4.10		
							0.10	0.14	0.04	−7.29			
							0.06	0.04	0.01	−23.32			
	1.09	2.00	2.82	12.72	0.02	71.57	0.33	0.10	0.01		0.60		
	3.91	2.43	4.43	10.36	0.01	83.90	0.66	0.74	3.62		8.50	−26.40	1.03
	0.54		2.19	12.03	0.00	71.32	0.03	0.06	0.01	22.11			
							0.03	0.06	0.00	−5.91			
							0.21	0.07	0.00	−25.65			
	0.58	1.29	2.87	13.17	0.01	33.39			0.01		—		
FB1a	0.32	1.38	3.34	11.29	0.01	50.59			0.01		—		
	0.32	2.08	4.31	15.62	0.02	53.85	0.15	0.56	0.00	−3.08	—		

—, below detection.